MAGNETOHYDRODYNAMICS Vol. 58 (2022), No. 4, pp. 545–553
DOI: 10.22364/mhd.58.4.19

CRUCIBLE CONSIDERATIONS IN INDUCTION FURNACE DEGASSING

J.C. Petrykowski

Vibration Heat Flow and Analysis LLP, Dayton, Ohio, USA 45459
e-Mail: jcpetrykowski@vhfaa.com

In a number of advanced materials processing applications, including float zone refining of electronic materials, forming of metallic glasses and induction melting of light alloys, oscillatory and non-oscillatory electromagnetic forces associated with the processing application are found to enhance surface shape, nucleation of precipitates, evolution of crystal nucleation sites, segregation of alloy components, grain refinement and degassing [1]–[3]. For cases where the material being processed is containerized and where the time dependence is oscillatory, these forces give rise to acoustic waves which carry energy to the boundaries of the containerized volume leading to a reduction in process efficacy should the container not present the proper acoustic impedance. This paper considers acoustic energy exchange between the molten alloy and the crucible of an induction furnace and the attendant impact on degassing.

Key words: Electromagnetic processing of materials, degassing, induction furnace

Introduction.

The paper (i) presents a model of the acoustic field in an induction furnace system, (ii) establishes crucible selection as a determinant for achieving proper distribution and retention of acoustic energy within the containerized volume, and (iii) identifies a set of operational parameters consistent with improved degassing action within slab and cylindrical induction furnace systems. To arrive at these stated objectives, we treat the acoustic field problem as an interaction between an inductively heated liquid melt in contact with an electrically nonconductive crucible. In both, the stress and velocity fields must satisfy the governing equations for mass and momentum, along with constitutive constraints for reversible, adiabatic, pressure-volume change. The discontinuity in material properties at the melt-crucible interface necessitates the introduction and use of nonorthogonal basis functions to represent the so-called nonorthogonal modes of vibration. A method is outlined for obtaining the amplitudes of these nonorthogonal modes through the use of an iso-energetic constraint. The vibrational energy of each component could then be obtained so that crucible selection may be informed by the energetic requirements of the degassing process. Mode shapes consistent with effective degassing are presented along with frequency constraints that establish optimal conditions for degassing. These frequency constraints are expressed as characteristic equations, the roots of which describe acoustic resonant frequencies of the system. For the slab, comparisons are made between the orthogonal (i.e. normal modes) and the nonorthogonal modes so as to delineate how the boundaries of the degassing zones are influenced, in a qualitative sense, by the characteristic acoustic impedance [4] of the crucible. Acoustic resonant frequencies are computed for slab and cylindrical melt degassing of aluminum and iron, respectively.

1. The magnetoacoustic problem.

Recent studies have examined acoustic degassing in an induction furnace from both an analytical and a finite element perspective [5–6]. In this paper, we extend the use of methodologies introduced in [5] to consider how refractory choice, of increasing importance in crucible design [7], may impact degassing effectiveness.

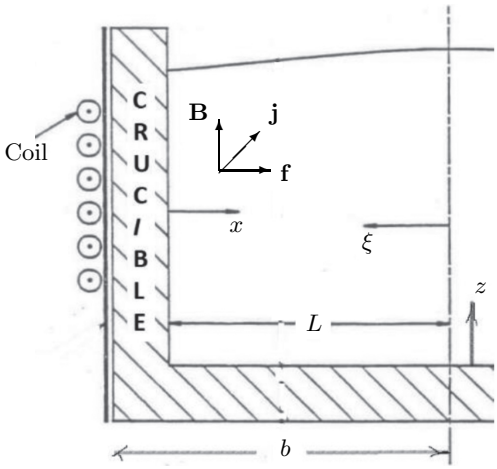

Fig. 1. Furnace, left-half view.

1.1. The slab furnace. Consider an inviscid liquid metal volume contained between planar, electrically nonconductive crucible walls (Fig. 1). A pair of inductors adjoining the crucible walls is supplied with alternating electric currents that are 180° out of phase so that both the secondary current and the body force within the layer are anti-symmetric about the midplane which then becomes a symmetry plane for the fluid motion. The electric currents are supplied at a sufficiently high frequency so that the electromagnetic depth of penetration, δ, may be considered as much smaller than $2L$, the thickness of the layer. Accordingly, the local electromagnetic field in the layer is induced solely by the nearest inductor. With these stipulations, the domain is reduced to a half-layer of thickness L positioned between a wall at $\xi = L$ and a symmetry plane at $\xi = 0$ with an inductor adjoined to the wall (Fig. 2).

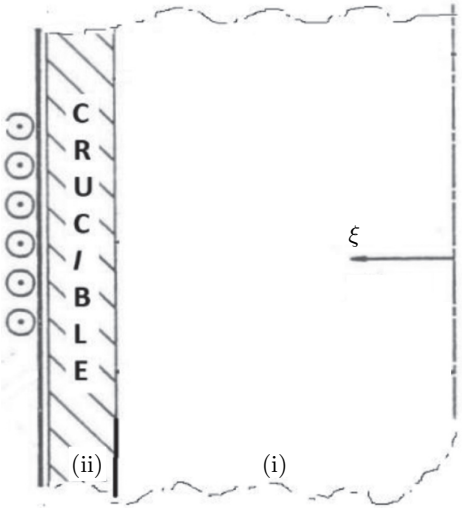

(ii): $b > \xi > L$, (i): $L > \xi > 0$, $\infty > z > -\infty$

Fig. 2. Furnace rendered as doubly-infinite parallel slabs; (i) melt, (ii) crucible.

The resulting electromagnetic field description for $\mathbf{B}$, the electromagnetic induction $\mathbf{E}$, the electric field and $\mathbf{j}$, the current density is determined by solving Maxwell's equations and Ohm's law which are

$$\boldsymbol{\nabla} \cdot \mathbf{B} = 0, \tag{1}$$

$$\mathbf{j} = \frac{1}{\mu} \boldsymbol{\nabla} \times \mathbf{B}, \tag{2}$$

$$\boldsymbol{\nabla} \times \mathbf{E} = -\frac{\partial \mathbf{B}}{\partial t}, \tag{3}$$

$$\mathbf{j} = \sigma \left(\mathbf{E} + \mathbf{V} \times \mathbf{B} \right), \tag{4}$$

where μ, σ, and $\mathbf{V}$ represent the magnetic permeability, the electrical conductivity and the velocity of the liquid metal. The response of the melt and the crucible to induced excitation is governed by the following linearized forms of the equations of continuity, motion and state

$$\frac{\partial \rho_1}{\partial t} + \rho_{01} \frac{\partial u_1}{\partial \xi} = 0, \tag{5}$$

$$\rho_{01} \frac{\partial u_1}{\partial t} = -\frac{\partial P_1}{\partial \xi} + (\mathbf{j} \times \mathbf{B})', \tag{6}$$

$$P_1 = \rho_1 c_1^2, \tag{7}$$

$$\frac{\partial \rho_2}{\partial t} + \rho_{02} \frac{\partial u_2}{\partial \xi} = 0, \tag{8}$$

$$\rho_{02} \frac{\partial u_2}{\partial t} = -\frac{\partial P_2}{\partial \xi}, \tag{9}$$

$$P_2 = \rho_2 c_2^2, \tag{10}$$

respectively, with ρ_0, ρ, u, P and c respresenting the dimensional representations for ambient density, excess density, velocity, acoustic pressure and sound speed for the 'slab' system, where subscripts 1 and 2 refer to the melt and the crucible, respectively, and where the primed symbol in (6) is used to denote the fluctuating part of $\mathbf{j} \times \mathbf{B}$.

The systems of equations (1)–(4) and (5)–(10) are inherently coupled by the nonlinear term in Eq. (4) which accounts for the dissipation of acoustic energy by currents generated as metal flows across magnetic field lines. As discussed in [5], this term may be omitted in many material processing applications thus permitting the electromagnetic and acoustic field problems to be solved separately leading to the following diffusion equation for the magnetic field:

$$\nabla^2 B = \mu \sigma \frac{\partial B}{\partial t}. \tag{11}$$

The solution to Eq. (11) for the present case of a harmonically varying field at a boundary of a conductive layer much thicker than the skin depth is given [8] by

$$B = B_0 \exp(-(L - \xi)/\delta) \cos(\omega t - (L - \xi)/\delta), \tag{12}$$

$$\delta = \sqrt{\frac{2}{\omega \sigma \mu}}, \tag{13}$$

where B_0 represents the field's peak strength which occurs at $\xi = L$. Then, the body force term in Eq. (6) is formed from Eqs. (12) and (2) as

$$(\mathbf{j} \times \mathbf{B})' = \frac{B_0^2}{\sqrt{2}\mu\delta} \cdot \exp\left[-\frac{2(L-\xi)}{\delta}\right] \cos\left[2\left(\omega t - \frac{L-\xi}{\delta}\right) + \frac{\pi}{4}\right]. \tag{14}$$

In section 1.2, we discuss the vibrational effect due to this excitation for a slab furnace configuration, while in section 2 we provide, in a comparative sense, acoustic resonant frequency values for typical melt-crucible combinations, some in three-dimensional cylindrical configurations.

1.2. Resonant acoustic frequency and mode shape solutions for the slab furnace problem. The mode shapes for both components are arrived at by recognizing, in the steady state, that the harmonic time dependence of the body force gives rise to a time harmonic response, so that the system (5)–(10) reduces to homogeneous and inhomogeneous Helmholtz equations governing the velocity and pressure mode shapes. Although nonorthogonal, the mode shapes must fit constraints at respective ends which are indicative of symmetry and compatibility at $\xi = 0$ and $\xi = L$, and compatibility and pressure release at $\xi = L$ and $\xi = b$. These constraints can be expressed as

$$u_1(L,t) = u_2(L,t), \tag{15}$$

$$u_1(0,t) = 0, \tag{16}$$

$$\left.\frac{\partial u_2}{\partial \xi}\right|_{\mathrm{b}} = 0, \tag{17}$$

where Eq. (17) is derived directly as a consequence of pressure release and conservation of mass. Impressing Eqs. (16)–(17) on the solutions leads to amplitude-weighted mode shape functions $(u_1^*, u_2^*, P_1^*, E_1^*)_i$ which describe the spatial variations of velocities, melt pressure and melt compressional energy [4] for the i-th mode of vibration. These functions are found to vary as

$$u_{1,i}^* \propto \sin K_{1,i}\xi, \tag{18}$$

$$u_{2,i}^* \propto \cos K_{2,i}(\xi - b), \tag{19}$$

$$P_{1,i}^* \propto \cos K_{1,i}\,\xi, \tag{20}$$

$$E_{1,i}^* \propto {P_{1,i}^*}^2 \propto \cos^2 K_{1,i}\,\xi, \tag{21}$$

where $K_{1,i} = 2\omega_i/c_1$ and $K_{2,i} = 2\omega_i/c_2$ are the wave numbers for the components. Asterisked variables, map to primitive variables viz., $u_{1,i} = u_{1,i}^* \cos 2\omega_{1,i} t$.

The resonant frequencies of distributed systems, for any i, can be found from characteristic equations [9]. Here, a characteristic equation, found by impressing Eq. (15) on Eqs. (18)–(19) leads to the transcendental form

$$\tan K_1 L = -\frac{\rho_{01} c_1}{\rho_{02} c_2}\left\{\frac{\cos K_2 L + \tan K_2 b \sin K_2 L}{\sin K_2 L - \tan K_2 b \cos K_2 L}\right\} \tag{22}$$

where $A \equiv (\rho_{01}c_1)/(\rho_{02}c_2)$ depends on the reciprocal characteristic impedances and so is referred to as the relative characteristic admittance of the crucible. Eq. (22) can be written as

$$F(K_2 b\,(c_2/c_1)\,(L/b)) = G(K_1 L; K_2 b) \tag{23}$$

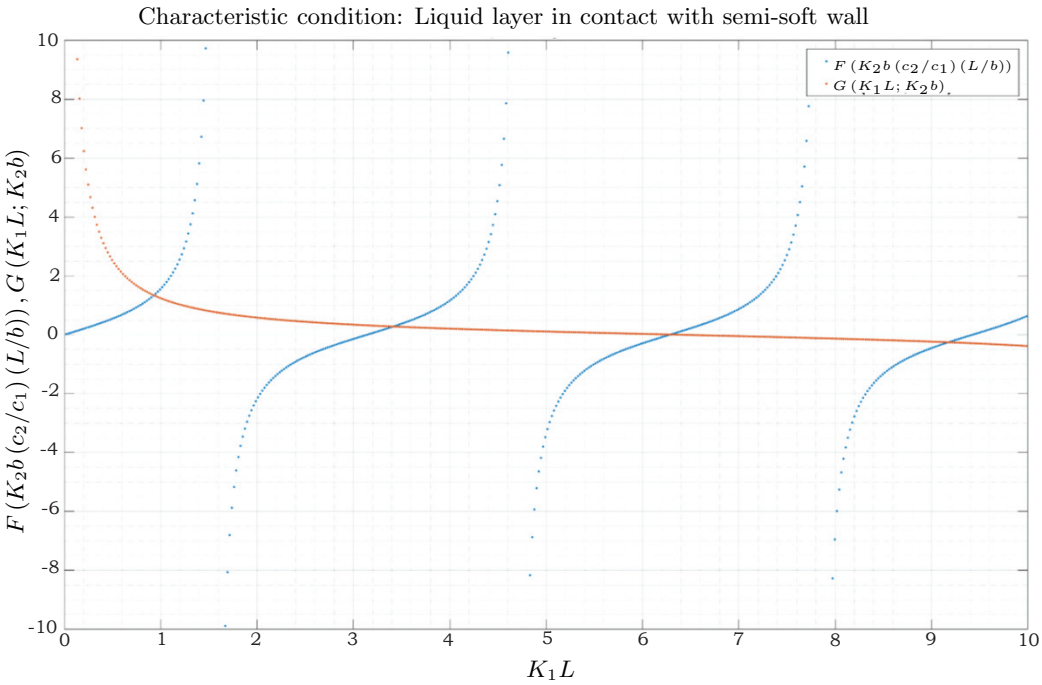

Fig. 3. Characteristic condition plot (any i) for slab furnace ($L = 0.225$ m, $b = 0.330$ m, aluminum melt, alumina crucible).

with $K_2 = c_1 K_1 / c_2$. Solutions of Eq. (23) are graphically depicted in Fig. 3, from which the first four roots for an aluminum-alumina, melt-crucible system can be found. The corresponding wave number-frequency pairs are

$$K_{1,i} L = \{0.926, 3.411, 6.281, 9.172 \ldots\} \tag{24}$$

$$\nu_i = \{3007, 11079, 20401, 29791\} \text{ [Hz]}. \tag{25}$$

Note that Eq. (22) also pertains to situations in which the crucible rigidity is quite large. For perfect rigidity, $\mathscr{A} = 0$, and Eq. (22) becomes $\sin K_1 L = 0$. The members of Eq. (24) are then multiples of π, and Eq. (18) becomes $u^*_{1,i} \propto \sin(i\pi\xi/L)$, which are the definitive velocity mode shapes for quiescent ends.

Finally, should the amplitude of vibration be needed, the electromagnetic body force contribution to the inhomogeneous Helmholtz equation is expanded using a set of basis functions so that coefficient multipliers can be inserted into Eqs. (18)–(21) following a left-hand side versus right-hand side matchup comparison. When the modes lack orthogonality, sets of candidate functions given by the likes of Eqs. (18)–(20) lack completeness and so a constraint is needed to allow the matchup process to proceed. An iso-energetic constraint, for any i, is chosen, which reads

$$\int_0^L \widehat{f}_{\mathrm{i}}^{\,\prime} u_{1,i} \mathrm{d}\xi = \int_0^L f^{\prime} u_{1,i} \mathrm{d}\xi \tag{26}$$

where $\widehat{f}_{\mathrm{i}}^{\,\prime}$ is the adjusted, fluctuating body force, whose action is energetically equivalent to $f^{\prime}$, the prescribed fluctuating body force given by Eq. (14). With $\widehat{f}_{\mathrm{i}}^{\,\prime}$ replacing the

prescribed body force, the matchup comparison can proceed without introducing loss in global representativeness of the vibrational energetics of the melt.

1.3. Equations for the 3D cylindrical furnace and solution of the frequency problem. With the geometry of most crucible induction furnace systems consistent with a closed-bottom vessel having circular cylindrical sides, we use a methodology developed for fluid-filled container vibrations to predict the vibrational characteristics of an inductively heated liquid iron charge held in a containment of christobolite. As a body of revolution, the side wall of a cylinder of height H is generally considered to be mechanically thin if the wall thickness h is more than an order of magnitude smaller than the cylinder radius a. If, in addition, wall properties can be characterized by uniform elastic constants E and ν, uniform mass density $\rho_{\rm s}$, and if boundary conditions at all melt surfaces can also be prescribed, then the vibrations of the liquid-wall system can be characterized, in part, as solutions of Eqs. (27), (30)–(32) [10],

$$c_1^{-2}\frac{\partial^2\phi}{\partial t^2}-\frac{1}{r}\frac{\partial\phi}{\partial r}-\frac{\partial^2\phi}{\partial r^2}-\frac{\partial^2\phi}{\partial z^2}=\frac{1}{\rho_{01}c_1^2}\frac{\partial}{\partial t}\frac{|\mathbf{B}^*|^2}{2\mu}, \tag{27}$$

$$\beta=\frac{h/a}{\sqrt{12}} \tag{28}$$

$$c_p=\left[\frac{E}{\rho_{\rm s}\left(1-\nu^2\right)}\right]^{1/2} \tag{29}$$

$$\frac{\nu}{a}\frac{\partial u}{\partial z}+\frac{1}{a^2}\frac{\partial v}{\partial\theta}-\beta^2\left(\frac{\partial^3 v}{\partial z^2\partial\theta}+\frac{1}{a^2}\frac{\partial^3 v}{\partial\theta^3}\right)+\frac{w}{a^2}+\beta^2a^2\left(\nabla^4 w\right)-\frac{\acute{w}}{c_{\rm p}^2}=p_{\rm a}\frac{1-\nu^2}{Eh}, \tag{30}$$

$$\frac{1+\nu}{2a}\frac{\partial^2 u}{\partial z\partial\theta}+\left(1+\beta^2\right)\left(\frac{1-\nu}{2}\frac{\partial^2 v}{\partial z^2}+\frac{1}{a^2}\frac{\partial^2 v}{\partial\theta^2}\right)+\frac{1}{a^2}\frac{\partial w}{\partial\theta}-\beta^2\left(\frac{\partial^3 w}{\partial z^2\partial\theta}+\frac{1}{a^2}\frac{\partial^3 w}{\partial\theta^3}\right)-\frac{\acute{v}}{c_{\rm p}^2}=0, \tag{31}$$

$$\frac{\partial^2 u}{\partial z^2}+\frac{1-\nu}{2a^2}\frac{\partial^2 u}{\partial\theta^2}+\frac{1+\nu}{2a}\frac{\partial^2 v}{\partial z\partial\theta}+\frac{\nu}{a}\frac{\partial w}{\partial z}-\frac{\acute{u}}{c_{\rm p}^2}=0, \tag{32}$$

$$\nabla^4=\frac{\partial^4}{\partial z^4}+2\frac{\partial^4}{a^2\partial z^2\partial\theta^2}+\frac{1}{a^4}\frac{\partial^4}{\partial\theta^4} \tag{33}$$

which govern ϕ, the velocity potential of the liquid in standard circular cylindrical coordinates, and u, v, w, the displacement triple for the wall in the respective wall coordinate directions z, θ and x.

Compatibility-type boundary conditions

$$\left.\frac{\partial w}{\partial t}\right|_{\rm a}=-\left.\frac{\partial\phi}{\partial r}\right|_{\rm a},\quad N_{\rm b}=P_{\rm a}a/2$$

are typical for side and bottom contact, respectively, but when extended to the top also require that $N_t=P_{\rm a}a/2$, where $N_{\rm b}$, N_t are the membrane stresses generally present in a closed induction furnace of the type used for vacuum melting of iron. Here $P_{\rm a}$ represents the ambient pressure. For details, the reader is referred to Berry and Reissner [11], who

Table 1. Resonant frequency characteristics for select crucible-melt configurations ($i=1$ case).

	Slab	Slab	$^{+}$Cylinder
Melt-Crucible	Al-Al_2O_3	*Fe-SiO_2	*Fe-SiO_2
ρ_{01}, [kg/m^3]	2300	7100	7100
ρ_{02}, [kg/m^3]	3900	2230	2230
E, [GPa]	30.3	62.3	62.3
G, [GPa]	125.0	32.4	32.4
c_1, [m/s]	4600	3800	3800
c_2, [m/s]	8701	5321	5321
c_{p}, [m/s]	–	–	5278
$\mathscr{A}$	0.312	2.304	2.304
ν_i, [Hz]	3002	6780	1707
$\nu_{\mathrm{p-rigid}}$, [Hz] ($\mathscr{A}=0$)	10204	16136	10742

$^{+}H=0.622$ m, *Cristobalite

obtained expressions for the wall displacement triple (u, v, w) as well as the following frequency formulations,

$$K = \acute{K_0}\sqrt{\lambda I_1(\lambda)/(\eta I_0(\lambda))} \tag{34}$$

with

$$\acute{K_0}^2 = 8/3 + \lambda^2\Omega/2 + (h\lambda^2/a)^2/4, \tag{35}$$

$$K = \omega a/c_{\mathrm{s}} \tag{36}$$

$$\eta = \rho_1 a/\rho_{\mathrm{s}} h \tag{37}$$

$$\lambda = \pi a/H \tag{38}$$

$$G = \frac{E}{2\,(1+\nu)}, \tag{39}$$

$$\Omega = P_{\mathrm{a}} \cdot (a/h)/G \tag{40}$$

in which K is the dimensionless fundamental frequency of resonant vibration and where I_0 and I_1 are the modified Bessel functions of the first kind, order zero and one, respectively.

2. Results and conclusions.

Resonant frequency conditions are now considered for aluminum and iron melts. Resonant frequency values are presented in Table 1 as a function of A, the relative characteristic admittance of the crucible, for both slab and cylindrical furnace configurations. Both zero characteristic admittance crucibles ("perfectly rigid") and finite admittance crucibles ("semi-soft") are considered. Regardless of melt composition, semi-soft crucibles bring about significant reductions in resonant frequency, with reductions ranging from 58 to 84%, thus emphasizing the importance of characterizing the properties of the crucible if an acoustic degassing campaign is planned.

Next, mode shapes presented in Fig. 4 depict, in a qualitative sense, the distribution of local perturbations from ambient, for pressure and acoustic energy. With regards to pressure, the trends capture the influence of wall rigidity; the magnitude of the pressure gradients at $\xi_{\mathrm{d}}=1$ lessens with decreasing admittance, trending towards the zero pressure gradient requirement of a quiesecent end. The acoustic energy modes indicate the distribution of zones of relatively high and relatively low "compressional" energy within the melt. A visual comparison of modes suggests that degassing zones are potentially

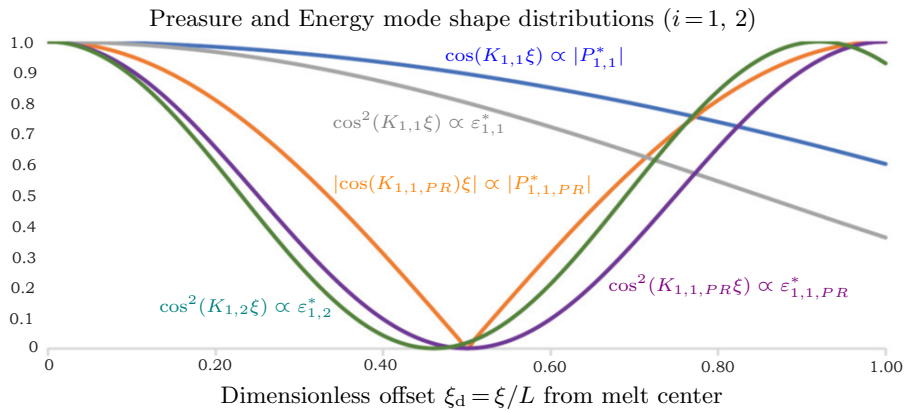

Fig. 4. Crucible effect on melt mode shapes in slab furnace. $L = 0.225$ m, $b = 0.330$ m, aluminum melt-alumina crucible, i.e., semi-soft wall; PR wall for comparison.

more extensive for the semi-soft case, through at least the first acoustical mode. These departures from estimates based on perfectly rigid crucible models [5] indicate that crucible contributions to melt acoustics must be accounted for, while highlighting challenges in designing efficient furnaces intended for both melting and degassing service.

References

[1] T. Tamura, Y. Maehara, N. Omura and K. Miwa. Motion of crystal particles by the electromagnetic vibrations in Mg-Cu-Y bulk metallic glasses. *Metallurgical and Materials Transactions A*, vol. 39 (2008), no. 8, pp. 1917–1921.

[2] S. Guo, Q. Le, Y. Han, Z. Zhao and J. Cui. The effect of the electromagnetic vibration on the microstructure, segregation, and mechanical properties of as-cast AZ80 magnesium alloy billet. *Metallurgical and Materials Transactions A*, vol. 37 (2006), no. 12, pp. 3715–3724.

[3] C. Vivès. Crystallization of aluminium alloys in the presence of cavitation phenomena induced by a vibrating electromagnetic pressure. *J. Crystal Growth*, vol. 158 (1996), pp. 118–127.

[4] J. Blitz. *Fundamentals of Ultrasonics* (2nd ed., Plenum Press, New York, NY, 1967).

[5] J.C. Petrykowski. Analysis of electromagnetically induced degassing in an induction furnace. In: *Proc. The 8th PAMIR International Conference on Fundamental and Applied MHD* (Borgo, Corsica, France, 2011), pp. 885–889.

[6] C.E.H. Tonry, G. Djambazov, A. Dybalska *et al.* Acoustic resonance for contactless ultrasonic cavitation in alloy melts. *Ultrasonics Sonochemistry*, vol. 63 (2020), pp.1–12.

[7] J.G. Hemrick, A. Rodrigues-Schroer, D. Colavito and J.D. Smith. Improved furnace efficiency through the use of refractory materials. *Light Metals*, vol. (2011), pp. 1211–1216.

[8] H.H. Woodson and J.R. Melcher. *Electromechanical Dynamics Part. 2* (Wiley, New York, NY, 1968).

[9] W.T. Thomson. *Theory of Vibrations with Applications* (2nd ed., Prentice Hall, Englewood Cliffs, NJ, 1981).

[10] M.C. Junger and D. Feit. *Sound, Structures and their Interactions* (1st ed., Ch. 9, MIT Press, Cambridge, MA, 1972).

[11] J.G. Berry and E. Reissner. The effect of an internal compressible fluid column on the breathing vibrations of a thin pressurized cylindrical shell. *J. Aerospace Sciences*, vol. 25 (1958), no. 5, pp. 288–294.

Received 04.10.2022